ELSEVIER

Journal of Organometallic Chemistry 492 (1995) 165–177

Journal of Organometallic Chemistry

# Photochemistry of the metal–metal-bonded complexes $[(CO)_5Mn–Ru(Me)(CO)_2(\alpha\text{-diimine})]$. Crystal structure of the photoproduct $[(CO)_4Mn\text{-}\mu\text{-}(\sigma(N),\sigma(N'),\eta^2(CN)\text{-}^i\text{Pr-PyCa})Ru(Me)(CO)_2]$

Heleen A. Nieuwenhuis [a], Annelies van Loon [a], Marieke A. Moraal [a], Derk J. Stufkens [a,*], Ad Oskam [a], Kees Goubitz [b]

[a] *Anorganisch Chemisch Laboratorium, Universiteit van Amsterdam, Nieuwe Achtergracht 166, 1018 WV Amsterdam, The Netherlands*
[b] *Laboratorium voor Kristallografie, Universiteit van Amsterdam, Nieuwe Achtergracht 166, 1018 WV Amsterdam, The Netherlands*

Received 10 August 1994

**Abstract**

Photochemical reactions are reported for the metal–metal-bonded complexes $[(CO)_5Mn–Ru(Me)(CO)_2(\alpha\text{-diimine})]$ [$\alpha$-diimine = pyridine-2-carbaldehyde-*N*-isopropylimine ($^i$Pr-PyCa), *N*,*N*′-diisopropyl-1,4-diaza-1,3-butadiene ($^i$Pr-DAB)] upon irradiation into their lowest-energy absorption band. The radicals $[Mn(CO)_5]^\cdot$ and $[Ru(Me)(CO)_2(\alpha\text{-diimine})]^\cdot$ are formed by homolytic splitting of the Mn–Ru bond; the latter radicals have been characterized by ESR spectroscopy. In THF, the $[Ru(Me)(CO)_2(^i\text{Pr-DAB})]^\cdot$ radicals dimerize to give $[Ru(Me)(CO)_2(^i\text{Pr-DAB})]_2$, and the corresponding radicals from the $^i$Pr–PyCa complex gave an unidentified product. Irradiation of a solution of the complexes in $CH_2Cl_2$ or $CHCl_3$ afforded $[Mn(Cl)(CO)_5]$ and $[Ru(Cl)(Me)(CO)_2(\alpha\text{-diimine})]$ but in apolar solvents such as hexane, completely different photoproducts, viz. $[(CO)_3Mn\text{-}\mu\text{-}(\sigma(N),\sigma(N'),\eta^2(CN),\eta^2(C'N')\text{-}^i\text{Pr-DAB})Ru(Me)(CO)_2]$ and $[(CO)_4Mn\text{-}\mu\text{-}(\sigma(N),\sigma(N'),\eta^2(CN)\text{-}^i\text{Pr-PyCa})Ru(Me)(CO)_2]$ were obtained. The crystal structure of the last complex was determined.

The photochemical quantum yield for the disappearance of the $^i$Pr-DAB complex was ca. 0.30, but only 0.05 for the $^i$Pr-PyCa complex. Low-temperature measurements and flash photolysis data showed that this difference in behaviour is due to the thermal instability of the dimer $[Ru(Me)(CO)_2(^i\text{Pr-PyCa})]_2$, which leads to partial regeneration of the parent complex at room temperature. At temperatures below 163 K, the photodecomposition into radicals was followed by electron transfer, leading to formation of the ions $[(CO)_5Mn]^-$ and $[Ru(Me)(S)(CO)_2(\alpha\text{-diimine})]^+$ in 2-MeTHF and the contact ion-pair $[(CO)_5Mn^- \cdots Ru(Me)(CO)_2(\alpha\text{-diimine})^+]$ in 2-chlorobutane. Similar photodisproportionation products were formed upon irradiation of the complexes at room temperature in the presence of N- or P-donor ligands.

*Keywords:* Manganese; Ruthenium; Metal–metal bonding; Photochemistry; Diimines; ESR spectroscopy

## 1. Introduction

Visible excitation of organometallic $\alpha$-diimine (bpy, phen, etc.) complexes can lead to the formation of radicals if the metal–$\alpha$-diimine moiety is covalently bonded to another metal fragment or an alkyl group; examples are the complexes $[L_nM–M'(CO)_3(\alpha\text{-diimine})]$ ($L_nM = (CO)_5Mn$, $(CO)_5Re$, $(CO)_4Co$, $Ph_3Sn$, etc.; M′ = Mn, Re) [1–8], $[Re(R)(CO)_3(\alpha\text{-diimine})]$ [9], $[Ru^I(^i\text{Pr})(CO)_2(^i\text{Pr-DAB})]$ [10] and $[Zn(R)_2(R'\text{-DAB})]$ [11]. With exception of the Zn compounds, all these complexes are characterized by strongly allowed metal-to-$\alpha$-diimine (MLCT) transitions in the visible region. Irradiation into these transitions gives rise to homolysis of the metal–metal or metal–alkyl bond and/or release of CO [1,8]. Release of CO has been observed only for the complexes $[L_nM–Mn(CO)_3(\alpha\text{-diimine})]$ [12,13]; this reaction probably occurs from a low-lying LF state, since it was also observed for the corresponding halide complexes $[Mn(X)(CO)_3(\alpha\text{-diimine})]$ [14]. The homolysis reactions, previously studied in detail

* Corresponding author.


*SSDI* 0022-328X(94)05300-6

for the above-mentioned metal–metal-bonded complexes $[L_nM-M'(CO)_3(\alpha\text{-diimine})]$ [1–6], proceeded with very high quantum yields (0.3–0.9). The radicals $[M'(CO)_3(\alpha\text{-diimine})]^{\cdot}$ could be detected by ESR spectroscopy, often without using a spin trap. In the presence of suitable nucleophiles such as $PR_3$, these radicals can initiate electron-transfer chain reactions.

Until recently, it has been unclear why excitation into a non-reactive MLCT state leads to such an efficient homolysis of the metal–metal bond. Studies of the complexes $[Re(R)(CO)_3(\alpha\text{-diimine})]$ [9] and $[Ru^I(R)(CO)_2(^i\text{Pr-DAB})]$ [10] (R = alkyl), for which the occurrence of the homolysis reaction strongly depends on R, have shown that these reactions probably occur from a $^3\sigma_b\pi^*$ state in which one electron has been transferred from the metal–alkyl bond to the $\alpha$-diimine. With exception of the $[Zn(R)_2(R'\text{-DAB})]$ [11] complexes, such a $\sigma_b \rightarrow \pi^*$ transition has never been observed for any of these metal–metal and metal–alkyl complexes. It has therefore been proposed that the reactive $^3\sigma_b\pi^*$ state is not reached by direct excitation into the corresponding $^1\sigma_b\pi^*$ state, but indirectly from the non-reactive MLCT states. A similar excited-state process was found for population of the D $\rightarrow \alpha$-diimine excited state of the chromophore-quencher complexes $[Re(D)(CO)_3(\alpha\text{-diimine})]^+$ (D = electron donor) [15–17].

We have recently prepared two complexes $[(CO)_5Mn-Ru(Me)(CO)_2(\alpha\text{-diimine})]$ [$\alpha$-diimine = pyridine-2-carbaldehyde-*N*-isopropylimine ($^i$Pr-PyCa) or *N*,*N*′-diisopropyl-1,4-diaza-1,3-butadiene ($^i$Pr-DAB)] (see Fig. 1) and studied their spectroscopic properties [18] and emission spectra at low temperature [19]. By the use of resonance Raman spectroscopy, the visible absorption band of these complexes was assigned to MLCT transitions [18]. In contrast, the emission of these $[(CO)_5Mn-Ru(Me)(CO)_2(\alpha\text{-diimine})]$ complexes in a 2-MeTHF glass at 77 K had a much longer lifetime and lower quantum yield than might be expected for a lowest MLCT state [19]. These long lifetimes and low quantum yields pointed to the presence of a lowest $^3\sigma_b\pi^*$ state, from which radiative transfer to the ground state is overlap-forbidden, and which has become occupied by surface crossing from the MLCT state(s).

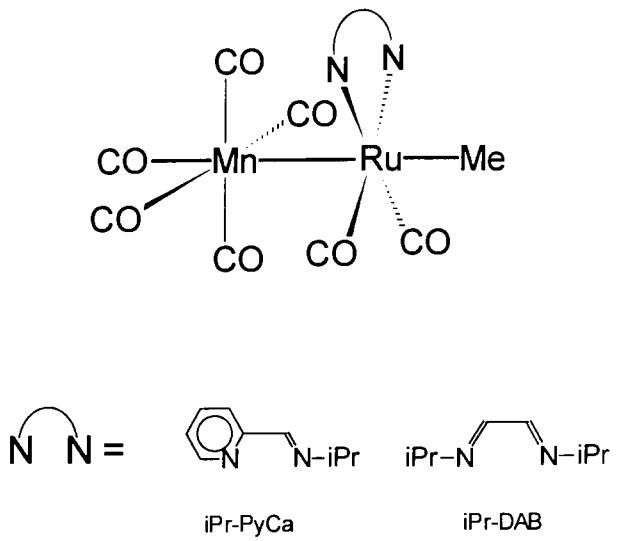


Fig. 1. Schematic formulae of $[(CO)_5Mn-Ru(Me)(CO)_2(\alpha\text{-diimine})]$ and of the ligands $^i$Pr-DAB and $^i$Pr-PyCa.

In this paper we report the photochemistry of these two $[(CO)_5Mn-Ru(Me)(CO)_2(\alpha\text{-diimine})]$ complexes. Special attention has been paid to the influence of the solvent on the product formation. The crystal structure of one of the photoproducts has been determined. The complexes under study are denoted below by MnRuDAB and MnRuPyCa and their formulae are shown in Fig. 1.

## 2. Experimental details

### 2.1. Materials

Solvents for synthetic purposes were of reagent grade, dried over sodium wire (THF, n-hexane) and freshly distilled under $N_2$. For spectroscopy, solvents of analytical grade [THF, n-hexane, 2-methyltetrahydrofuran (2-MeTHF), $CH_2Cl_2$] or UVASOL quality (toluene) were used. They were dried over sodium wire, except for $CH_2Cl_2$ and 2-chlorobutane, which were dried over $CaCl_2$ and distilled under nitrogen prior to use. Paraffin was used without further purification. All preparations were performed under purified nitrogen, using Schlenk techniques. The photosensitive compounds were carefully handled with exclusion of light. $P(^nBu)_3$ and $P(OPh)_3$ were distilled from $CaH_2$ and stored under nitrogen; $PPh_3$ was recrystallized from n-hexane; $NEt_3$ was distilled from KOH and stored under nitrogen; pyridine was used as received.

### 2.2. Apparatus and photochemistry

Infrared spectra were recorded on a Nicolet 7199 B FT-IR or BioRad FTS-7 FT-IR spectrophotometer. Electronic absorption spectra were recorded on a Perkin-Elmer Lambda 5 UV–vis spectrophotometer, equipped with a 3600 Data Station or a Varian Cary 4E spectrophotometer. $^1$H NMR spectra were recorded on a Bruker AC-100 or AMX-300 spectrometer. ESR measurements were performed on a Varian E6 ESR spectrometer with a temperature accessory. Coupling constants were obtained by computer simulation. Low-temperature UV–vis and IR studies were carried out using an Oxford Instruments DN 1704/54 liquid nitrogen cryostat.

For the photochemical reactions the complexes were irradiated with one of the lines of an SP 2025 argon ion laser or a Philips HPK 125 W high-pressure mercury lamp fitted with the appropriate interference filter.

Quantum yields were measured on a Varian Cary 4E spectrophotometer with automatized procedures. The thermostatted cuvettes containing the sample solutions were kept in the UV–vis spectrophotometer during the measurements. Using an optical fibre and a computer-controlled mechanical shutter, the stirred sample was irradiated with one of the laser lines of an SP 2025 argon ion laser. The light intensities were measured with a power meter, which was calibrated with an Aberchrome 540 solution by standard methods [20]. Quantum yields were determined by following the decay of the parent MLCT band.

For the nanosecond flash photolysis studies, the sample was excited by flashes of a Nd:YAG laser (Spectra Physics GCR-3; 10 ns pulse width) at 532 nm wavelength. A 450 W high-pressure Xe lamp was used as the probe light, pulsed by a Müller Elektronik MSPO5 pulser. After passing through the sample, the probe light was collected into a fibre and transferred to a spectrograph (EG & G model 1234) equipped with a 150 g $mm^{-1}$ grating and a 250 micrometer slit resulting in a resolution of 6 nm. This spectrograph was coupled to a gated, intensified diode array detector (EG & G model 1421) which was part of an EG & G OMA III handling system and a 1304 Gate Pulse Amplifier with variable time windows of 100 ns to 10 ms. The programming of the OMA led to a time-resolved measurement. During the photolysis experiment, the sample flowed through a homebuilt cell, which was especially developed for detection of short-lived intermediates and which operated under inert gas atmosphere.

### 2.3. Preparation of the complexes

The two complexes MnRuDAB and MnRuPyCa were prepared by previously described methods [18].

Photoproduct A was prepared by irradiation with 514.5 nm ($P = 300$ mW) of a 1 mmol solution of MnRuPyCa in 100 ml of THF under nitrogen atm for several hours. The progress of the reaction was monitored by IR spectroscopy. The solution was evaporated to dryness and the product purified by washing with hexane. IR $\nu$(CO) (THF) ($cm^{-1}$): 2023, 1952; UV–vis (THF) (nm): 368, 547; $^1$H NMR (MeOD)$\delta$: 8.83 (2H, d); 8.14 (2H, d); 7.76 (2H, d/s); 4.23 (1H, m); 1.49 (6H, s/m); 0.66 (1H, dd); −0.037 (1H, s) ppm.

Photoproducts [$(CO)_3$Mn-$\mu$-($\sigma$(N),$\sigma$(N'),$\eta^2$(CN), $\eta^2$(C'N')-$^i$Pr-DAB)Ru(Me)$(CO)_2$] and [$(CO)_4$Mn-$\mu$-($\sigma$(N),$\sigma$(N'),$\eta^2$(CN)-$^i$Pr-PyCa)Ru(Me)$(CO)_2$] were prepared by careful irradiation of MnRuDAB or MnRuPyCa in hexane solution with 514.5 nm light. Washing with n-hexane yielded the photoproduct, which was purified by column chromatography on an activated silica column with n-hexane as eluent and finally recrystallized from hexane.

$^i$Pr-DAB: IR $\nu$(CO) (hexane)($cm^{-1}$): 2032, 2007, 1957, 1937, 1932; UV–vis (THF)(nm): 345; $^1$H NMR ($CDCl_3$)$\delta$: 6.03 (2H, s); 2.57 (3H, s); 2.37 (2H, m); 1.14 (3H, d); 1.06 (3H, d) ppm.

$^i$Pr-PyCa: IR $\nu$(CO) (THF)($cm^{-1}$): 2046, 2013, 1967, 1935, 1889; UV–vis (THF)(nm); 309, 388; $^1$H NMR ($CDCl_3$)$\delta$: 8.11 (1H, d); 7.39 (2H, dd); 6.79 (1H, t); 5.11 (1H, s); 2.94 (1H, m); 1.55 (3H, d); 1.31 (3H, d); −0.52 (3H, s) ppm.

Table 1
Crystallographic data for [$(CO)_4$Mn-$\mu$-($\sigma$(N),$\sigma$(N'),$\eta^2$(CN)-$^i$Pr-PyCa)Ru(Me)$(CO)_2$]

| | |
|---|---|
| Formula | $C_{16}H_{15}MnN_2O_6Ru$ |
| Molecular weight | 487.3 |
| Space group | triclinic, $P\bar{1}$ |
| $a, b, c$ (Å) | 9.049(1), 13.866(1), 16.756(1) |
| $\alpha, \beta, \gamma$ (°) | 106.394(8), 103.942(11), 97.661(7) |
| $V$ (Å$^3$) | 2049.1(4) |
| $Z$ | 4 |
| $D_x$ (g $cm^{-1}$) | 1.69 |
| $\lambda$(Cu K$\alpha$) (Å) | 1.5418 |
| $\mu$(Cu K$\alpha$) ($cm^{-1}$) | 122.76 |
| $F$(000) | 968 |
| Temperature (K) | 293 |
| Final $R$, $R_w$ | 0.048, 0.065 |
| Observed reflections | 6242 |

### 2.4. Crystal structure of [$(CO)_4$Mn-$\mu$-($\sigma$(N),$\sigma$(N'), $\eta^2$(CN)-$^i$Pr-PyCa)Ru(Me)$(CO)_2$]

The crystallographic data for [$(CO)_4$Mn-$\mu$-($\sigma$(N),$\sigma$(N'),$\eta^2$(CN)-$^i$Pr-PyCa)Ru(Me)$(CO)_2$] are listed in Table 1. A crystal of dimensions ca. 0.25 × 0.45 × 0.60 mm was used for data collection on an Enraf-Nonius CAD4 diffractometer with graphite-monochromated Cu K$\alpha$ radiation and an $\omega$–2$\theta$ scan. A total of 7211 unique reflections was measured within the range $-10 \le h \le 11$, $-16 \le k \le 0$, $-19 \le l \le 20$. Of these, 6242 were above the significance level of 2.5 $\sigma(I)$.

The maximum value of (sin $\theta$)/$\lambda$ was 0.61 Å$^{-1}$. Two reference reflections (224, 211) were measured hourly and showed a 9% decrease during the 80 h collection time, and correction was made for this. Unit cell parameters were refined by a least-squares fitting procedure using 23 reflections with $80 < 2\theta < 82°$. Corrections for Lorentz and polarization effects were applied. The heavy atoms were found by direct methods. The remaining non-hydrogen atoms were found in a subsequent $\Delta F$ synthesis. The hydrogen atoms were placed in calculated positions. Full-matrix least-squares refinement on $F$, anisotropic for the non-hydrogen atoms and isotropic for the hydrogen atoms, with the latter constrained in such a way that the distance to their

carrier remained constant at approximately 1.09 Å, converged to $R = 0.048$, $R_w = 0.065$, $(\Delta/\sigma)_{max} = 0.56$. A weighting scheme $w = (10.0 + F_{obs} + 0.0063F_{obs}^2)$ was used. An empirical absorption correction (DIFABS) [21] was applied, with coefficients in the range 0.69–1.64. The secondary isotropic extinction coefficient [22,23] refined to $G = 0.019(5)$. A final difference Fourier map revealed a residual electron density between −2.4 and 1.6 e $Å^{-3}$ in the vicinity of the heavy atoms. There are two identical independent molecules in the asymmetric unit. Matching those two molecules, with omission of the hydrogen atoms, led to an RMS value of 0.23 Å. Scattering factors were taken from Cromer and Mann [24] and from *International Tables for X-ray Crystallography* [25]. The anomalous scattering of Mn and Ru was taken into account. All calculations were performed with XTAL [26], unless stated otherwise. Tables of anisotropic thermal parameters and hydrogen atom coordinates and complete lists of bond lengths and angles have been deposited at the Cambridge Crystallographic Data Centre.

## 3. Results

### 3.1. Photochemical reactions at room temperature

The photochemistry of the two complexes MnRuDAB and MnRuPyCa was studied in various solvents and at temperatures between 133 K and room temperature. The reactions were monitored in situ by IR and UV–vis spectroscopy and the spectral data for the photoproducts are listed in Table 2 and in Tables 7 and 8 below.

Both complexes reacted thermally with $CCl_4$ to give $[Mn(Cl)(CO)_5]$ and $[Ru(Cl)(Me)(CO)_2(\alpha\text{-diimine})]$. In $CH_2Cl_2$ and $CHCl_3$, these products could only be obtained photochemically by irradiation into the MLCT band. The occurrence of this reaction points to a light-induced homolysis of the metal–metal bond with formation of the radicals $[Mn(CO)_5]^{\cdot}$ and $[Ru(Me)(CO)_2(\alpha\text{-diimine})]^{\cdot}$.

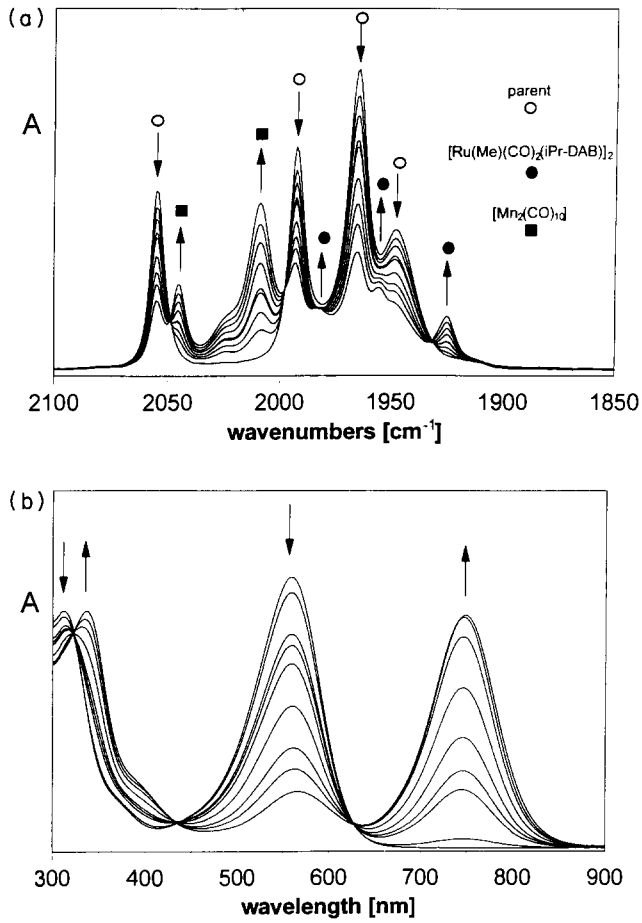


Fig. 2. (a) IR and (b) UV–vis spectral changes during photolysis of MnRuDAB in THF at room temperature.

The splitting into radicals was also evident from the photodecomposition of MnRuDAB in THF, which gave rise to the dimeric species $[Mn_2(CO)_{10}]$ and $[Ru(Me)(CO)_2(^iPr\text{-DAB})]_2$. Fig. 2 shows the IR and UV–vis spectral changes accompanying this photoreaction. The

Table 2
IR and UV–vis data of the photoproducts obtained in various solvents at room temperature [$\nu$(CO) in $cm^{-1}$; $\lambda_{max,abs}$ in nm]

| Product | $\nu$(CO) | $\lambda_{max,abs}$ | Main product in |
|---|---|---|---|
| $[Mn_2(CO)_{10}]$ | 2045 (m), 2009 (s) [a] | 340 | THF, toluene |
| $[Ru(Me)(CO)_2(^iPr\text{-DAB})]_2$ | 1982 (m), 1957 (s), 1923 (s) [a] | 750 | THF, toluene |
| Photoproduct A | 2023 (s), 1952 (s) [a] | 368, 547 | THF, toluene |
| $[(CO)_3Mn\text{-}\mu\text{-}(\sigma(N),\sigma(N'),\eta^2(CN),\eta^2(C'N')\text{-}^iPr\text{-DAB})Ru(Me)(CO)_2]$ | 2032 (m), 2007 (s), 1957 (m) | 345 | hexane, parafin |
| | 1937 (m), 1932 (m) [b] | | PVC |
| $[(CO)_4Mn\text{-}\mu\text{-}(\sigma(N),\sigma(N'),\eta^2(CN)\text{-}^iPr\text{-PyCa})Ru(Me)(CO)_2]$ | 2051 (m), 2019 (s), 1976 (s), | 309, 388 | hexane |
| | 1949 (m), 1901 (m/w) [b] | | |
| $[Mn(Cl)(CO)_5]$ | 2056 (vs), 2000 (m) | | $CH_2Cl_2$, $CHCl_3$ |
| $[Ru(Cl)(Me)(CO)_2(^iPr\text{-DAB})]$ | 2032 (s), 1958 (s) [c] | 435 | $CH_2Cl_2$, $CHCl_3$ |
| $[Ru(Cl)(Me)(CO)_2(^iPr\text{-PyCa})]$ | 2030 (s), 1957 (s) [c] | 360 | $CH_2Cl_2$, $CHCl_3$ |

[a] Measured in THF.
[b] Measured in hexane.
[c] Measured in $CH_2Cl_2$.

parent absorption band at 558 nm disappears and two new bands show up at ca. 340 and 745 nm, respectively. These bands are characteristic for the products $[Mn_2(CO)_{10}]$ [27] and $[Ru(Me)(CO)_2(^iPr\text{-}DAB)]_2$ [28]. The assignment is confirmed by the appearance of the well-known CO stretching frequencies for these photoproducts [27,28].

In the case of the complex MnRuPyCa, the results in THF were somewhat different. Again, the 585 nm band disappeared and the formation of $[Mn_2(CO)_{10}]$ was evident from the IR spectra. However, the $[Ru(Me)(CO)_2(^iPr\text{-}PyCa)]^{\cdot}$ radicals did not give rise to a metal–metal-bonded dimer, as in the case of MnRuDAB, since no characteristic low-energy absorption was observed. The Ru radicals were not present as such in solution, since a spectroelectrochemical study has shown that the $\nu$(CO) frequencies for these radicals in THF are 2000 and 1940 $cm^{-1}$ [29], whereas the photoproduct exhibits CO stretching frequencies at 2023 and 1952 $cm^{-1}$ in this solvent. Since these frequencies closely resemble those for the corresponding mononuclear halide complexes $[Ru(X)(Me)(CO)_2(^iPr\text{-}PyCa)]$ (X = halide), it is possible that the radicals reacted with solvent molecules to give $[Ru(H)(Me)(CO)_2(^iPr\text{-}PyCa)]$ but, the IR and $^1H$ NMR spectra did not show the formation of such a hydride. Importantly, the imine proton had disappeared from the $^1H$ NMR spectra and the mass spectrum of this photoproduct, denoted by A, showed a weak signal at $m/z$ 512. These data point to the formation of a carbon–carbon coupling product from two $[Ru(Me)(CO)_2(^iPr\text{-}PyCa)]^{\cdot}$ radicals or to a dinuclear structure in which the $^i$Pr-PyCa ligand is isomerized by transferring a proton of the $^i$Pr group to the imine fragment [30]. Recently, such a C–C-coupled dimer has been obtained by reduction $[Re(Br)(CO)_3(^iPr\text{-}PyCa)]$ and characterized by a crystal structure determination [9]. It has not been possible to determine the structure of this photoproduct A by an X-ray diffraction study.

The solvent had a large influence on the product formation since the main products formed in hexane were different from those formed in THF. Hardly any $[Mn_2(CO)_{10}]$ was produced in hexane and the photoreaction was even accelerated by addition of extra $[Mn_2(CO)_{10}]$ to the solution, especially when shorter wavelengths were used for irradiation. Apparently, $[Mn(CO)_5]^{\cdot}$ radicals formed by irradiation of $[Mn_2(CO)_{10}]$ were involved in the product formation. The photoproduct was therefore expected to contain both an Mn and an Ru fragment and this was confirmed by a crystal structure determination of the photoproduct from the MnRuPyCa complex (vide infra). In viscous media such as paraffin and PVC, the photoproducts were similar to those formed in hexane. The spectral

Table 3
Atomic coordinates (Å) for the two independent molecules (A and B) of $[(CO)_4Mn\text{-}\mu\text{-}(\sigma(N),\sigma(N'),\eta^2(CN)\text{-}^iPr\text{-}PyCa)Ru(Me)(CO)_2]$ with esds in parentheses

| Atom | Molecule A | | | | Molecule B | | | |
|---|---|---|---|---|---|---|---|---|
| | $x$ | $y$ | $z$ | $U_{eq}$ (Å$^2$) | $x$ | $y$ | $z$ | $U_{eq}$ (Å$^2$) |
| Ru(1) | 1.19665(4) | −0.11801(3) | 0.25657(2) | 0.0244(2) | 0.66011(5) | 0.33194(3) | 0.22628(3) | 0.0269(2) |
| Mn(1) | 0.93107(9) | −0.03741(6) | 0.26643(5) | 0.0236(4) | 0.5355(1) | 0.50469(7) | 0.21839(6) | 0.0330(5) |
| C(1) | 1.1060(6) | 0.0732(4) | 0.2608(4) | 0.027(3) | 0.7603(7) | 0.5494(4) | 0.3055(4) | 0.035(3) |
| C(2) | 1.1560(6) | 0.0473(4) | 0.1828(3) | 0.027(3) | 0.7716(7) | 0.5140(5) | 0.3799(4) | 0.036(3) |
| C(3) | 1.1507(7) | 0.1064(5) | 0.1270(4) | 0.042(4) | 0.807(1) | 0.5802(6) | 0.4654(5) | 0.058(4) |
| C(4) | 1.2047(9) | 0.0767(7) | 0.0569(5) | 0.060(5) | 0.813(1) | 0.5370(9) | 0.5319(5) | 0.082(6) |
| C(5) | 1.2662(9) | −0.0116(7) | 0.0410(5) | 0.059(5) | 0.779(1) | 0.4308(9) | 0.5116(5) | 0.072(6) |
| C(6) | 1.2676(8) | −0.0671(6) | 0.0968(4) | 0.042(3) | 0.7481(8) | 0.3724(7) | 0.4277(5) | 0.051(4) |
| C(7) | 1.2269(7) | 0.0955(5) | 0.4134(4) | 0.040(3) | 0.8546(7) | 0.5132(6) | 0.1779(5) | 0.045(4) |
| C(8) | 1.384(1) | 0.1603(7) | 0.4252(6) | 0.068(5) | 1.0233(9) | 0.5123(8) | 0.2214(7) | 0.065(5) |
| C(9) | 1.237(1) | 0.0366(7) | 0.4771(4) | 0.063(5) | 0.804(1) | 0.4504(9) | 0.0839(6) | 0.074(6) |
| C(10) | 1.4458(7) | −0.0908(6) | 0.2992(5) | 0.048(4) | 0.8610(8) | 0.2680(5) | 0.2344(6) | 0.053(4) |
| C(11) | 1.2037(8) | −0.2441(5) | 0.1817(4) | 0.043(4) | 0.5654(7) | 0.2116(5) | 0.2395(4) | 0.038(3) |
| C(12) | 1.1841(8) | −0.1817(5) | 0.3394(4) | 0.044(4) | 0.5917(9) | 0.2656(5) | 0.1066(5) | 0.050(4) |
| C(13) | 0.8737(7) | 0.0573(4) | 0.3495(4) | 0.035(3) | 0.5645(9) | 0.6019(6) | 0.1631(5) | 0.056(4) |
| C(14) | 0.8513(7) | −0.1350(5) | 0.3063(4) | 0.037(3) | 0.3755(9) | 0.4377(7) | 0.1205(5) | 0.059(4) |
| C(15) | 0.7621(7) | −0.0287(5) | 0.1875(4) | 0.039(3) | 0.4569(8) | 0.5937(5) | 0.2879(5) | 0.051(4) |
| C(16) | 0.9313(7) | −0.1476(5) | 0.1685(4) | 0.037(3) | 0.4433(7) | 0.4071(5) | 0.2614(4) | 0.041(3) |
| N(1) | 1.1626(5) | 0.0252(3) | 0.3225(3) | 0.024(2) | 0.7523(5) | 0.4768(3) | 0.2268(3) | 0.029(2) |
| N(2) | 1.2129(5) | −0.0383(4) | 0.1662(3) | 0.028(2) | 0.7411(6) | 0.4117(4) | 0.3622(3) | 0.034(2) |
| O(11) | 1.2090(8) | −0.3198(4) | 0.1333(4) | 0.074(4) | 0.5138(6) | 0.1389(4) | 0.2504(4) | 0.065(3) |
| O(12) | 1.1760(8) | −0.2253(5) | 0.3884(4) | 0.076(4) | 0.5466(9) | 0.2191(5) | 0.0343(4) | 0.087(4) |
| O(13) | 0.8305(7) | 0.1120(4) | 0.3977(4) | 0.062(3) | 0.5681(9) | 0.6599(6) | 0.1286(5) | 0.095(6) |
| O(14) | 0.7989(7) | −0.1959(4) | 0.3310(4) | 0.066(4) | 0.2692(9) | 0.3981(7) | 0.0622(5) | 0.112(5) |
| O(15) | 0.6592(6) | −0.0231(6) | 0.1359(4) | 0.070(4) | 0.4142(8) | 0.6496(5) | 0.3382(5) | 0.081(4) |
| O(16) | 0.8797(6) | −0.2098(4) | 0.1020(3) | 0.066(3) | 0.3562(6) | 0.3694(5) | 0.2891(4) | 0.066(4) |

Table 4
Selected bond distances (Å) in the two independent molecules (A and B) of [$(CO)_4$Mn-$\mu$-($\sigma$(N),$\sigma$(N'),$\eta^2$(CN)-$^i$Pr-PyCa)Ru(Me)$(CO)_2$] with esds in parentheses

| Bonds | Distance (A) | Distance (B) | Bonds | Distance (A) | Distance (B) |
|---|---|---|---|---|---|
| Ru(1)–Mn(1) | 2.803(1) | 2.803(1) | Mn(1)–C(15) | 1.807(6) | 1.791(8) |
| Ru(1)–C(10) | 2.140(6) | 2.118(8) | Mn(1)–C(16) | 1.901(6) | 1.895(8) |
| Ru(1)–C(11) | 1.862(6) | 1.868(7) | Mn(1)–N(1) | 2.033(4) | 2.030(5) |
| Ru(1)–C(12) | 1.859(8) | 1.860(7) | C(11)–O(11) | 1.146(9) | 1.133(9) |
| Ru(1)–N(1) | 2.085(4) | 2.066(5) | C(12)–O(12) | 1.16(1) | 1.141(9) |
| Ru(1)–N(2) | 2.131(5) | 2.122(4) | C(13)–O(13) | 1.126(9) | 1.12(1) |
| Mn(1)–C(1) | 2.091(6) | 2.092(5) | C(14)–O(14) | 1.14(1) | 1.134(9) |
| Mn(1)–C(13) | 1.852(6) | 1.86(1) | C(15)–O(15) | 1.136(8) | 1.15(1) |
| Mn(1)–C(14) | 1.811(7) | 1.812(6) | C(46)–O(16) | 1.142(7) | 1.14(1) |

data for the photoproducts obtained in various solvents are listed in Table 2.

### 3.2. Crystal structure of [$(CO)_4$Mn-$\mu$-($\sigma$(N),$\sigma$(N'), $\eta^2$(CN)-$^i$Pr-PyCa)Ru(Me)$(CO)_2$]

Fig. 3 shows the molecular structure of the photoproduct obtained from MnRuPyCa in apolar solution. The main difference between the parent complex [$(CO)_5$Mn–Ru(Me)$(CO)_2$($\sigma$(N),$\sigma$(N')–$^i$Pr–PyCa)] and this photoproduct [$(CO)_4$Mn-$\mu$-($\sigma$(N),$\sigma$(N'),$\eta^2$(CN)–$^i$Pr–PyCa)Ru(Me)$(CO)_2$] is in the replacement of a CO ligand of the $Mn(CO)_5$ moiety by the imine group of the $^i$Pr-PyCa ligand. Similar substitution products have been obtained upon photolysis of [$(CO)_5$Mn–$Mn(CO)_3$($^i$Pr-PyCa)] [6], [$Cp(CO)_2$Fe–$Re(CO)_3$($^i$Pr–PyCa)] [31] and [$(CO)_5$Mn–$Mn(CO)_3$(DBSD)] (DBSD = di-t-butylsulphurdiimine) [32] in apolar and viscous media.

The fractional coordinates, selected bond lengths and selected bond angles for the photoproduct are listed in Tables 3, 4 and 5, respectively. The complex contains an Mn and an Ru fragment connected by a metal–metal bond of length 2.80 Å, which is shorter than the corresponding bond in the parent complex (2.99 Å) [18]. In addition, the $^i$Pr–PyCa ligand now forms a bridge between the two metal fragments, being $\sigma$(N1)- $\sigma$(N2)-bonded to Ru and $\eta^2$-(C1–N1) to Mn. As a result of the extra $\eta^2$-bond, the ligand has lost its planar skeleton and the imine group makes an angle of 17° with the plane of the pyridine ring. With respect to the parent complex, the angle between the metal–metal and metal–alkyl bond has decreased from 180° to 147°. The Ru–carbonyl and Ru–methyl bond lengths are

Table 5
Selected bond angles (°) in the two independent molecules (A and B) of [$(CO)_4$Mn-$\mu$-($\sigma$(N),$\sigma$(N'),$\eta^2$(CN)-$^i$Pr-PyCa)Ru(Me)$(CO)_2$] with esds in parentheses

| Bonds | Angle (A) | Angle (B) | Bonds | Angle (A) | Angle (B) |
|---|---|---|---|---|---|
| Mn(1)–Ru(1)–C(10) | 146.7(2) | 146.2(2) | C(1)–Mn(1)–C(14) | 155.4(2) | 159.9(3) |
| Mn(1)–Ru(1)–C(11) | 127.0(2) | 127.9(2) | C(1)–Mn(1)–C(15) | 101.9(3) | 94.4(3) |
| Mn(1)–Ru(1)–C(12) | 93.7(2) | 94.6(2) | C(1)–Mn(1)–C(16) | 98.2(3) | 99.8(3) |
| Mn(1)–Ru(1)–N(1) | 46.3(1) | 46.3(1) | C(1)–Mn(1)–N(1) | 40.0(2) | 39.5(2) |
| Mn(1)–Ru(1)–N(2) | 85.1(1) | 84.2(2) | C(13)–Mn(1)–C(14) | 87.1(3) | 84.2(4) |
| C(10)–Ru(1)–C(11) | 86.1(3) | 85.6(3) | C(13)–Mn(1)–C(15) | 86.9(3) | 87.8(4) |
| C(10)–Ru(1)–C(12) | 90.5(3) | 90.0(3) | C(13)–Mn(1)–C(16) | 164.6(2) | 163.0(3) |
| C(10)–Ru(1)–N(1) | 100.4(2) | 100.0(3) | C(13)–Mn(1)–N(1) | 93.4(2) | 93.0(3) |
| C(10)–Ru(1)–N(2) | 89.2(3) | 90.2(3) | C(14)–Mn(1)–C(15) | 102.7(3) | 105.6(4) |
| C(11)–Ru(1)–C(12) | 88.4(3) | 88.2(3) | C(14)–Mn(1)–C(16) | 86.7(3) | 83.3(4) |
| C(11)–Ru(1)–N(1) | 170.5(3) | 171.3(3) | C(14)–Mn(1)–N(1) | 115.4(2) | 120.4(3) |
| C(11)–Ru(1)–N(2) | 94.2(3) | 93.5(2) | C(15)–Mn(1)–C(16) | 80.8(3) | 84.5(4) |
| C(12)–Ru(1)–N(1) | 98.3(3) | 98.5(3) | C(15)–Mn(1)–N(1) | 141.9(3) | 133.8(2) |
| C(12)–Ru(1)–N(2) | 177.3(2) | 178.3(3) | C(16)–Mn(1)–N(1) | 102.0(2) | 103.2(3) |
| N(1)–Ru(1)–N(2) | 79.1(2) | 79.8(2) | Ru(1)–C(11)–O(11) | 177.2(8) | 176.9(6) |
| Ru(1)–Mn(1)–C(1) | 70.0(2) | 69.4(2) | Ru(1)–C(12)–O(12) | 177.1(6) | 175.4(8) |
| Ru(1)–Mn(1)–C(13) | 136.6(2) | 133.7(3) | Mn(1)–C(16)–O(16) | 156.2(6) | 158.0(6) |
| Ru(1)–Mn(1)–C(14) | 93.1(2) | 96.0(3) | Ru(1)–N(1)–Mn(1) | 85.8(1) | 86.4(2) |
| Ru(1)–Mn(1)–C(15) | 134.7(2) | 135.3(3) | Ru(1)–N(1)–C(1) | 108.4(3) | 109.2(4) |
| Ru(1)–Mn(1)–C(16) | 57.9(2) | 59.4(2) | Mn(1)–N(1)–C(1) | 72.2(3) | 72.7(3) |
| Ru(1)–Mn(1)–N(1) | 47.9(1) | 47.4(1) | Ru(1)–N(2)–C(2) | 112.4(4) | 111.9(4) |
| C(1)–Mn(1)–C(13) | 93.2(3) | 95.9(3) | Ru(1)–N(2)–C(6) | 127.2(5) | 128.1(4) |

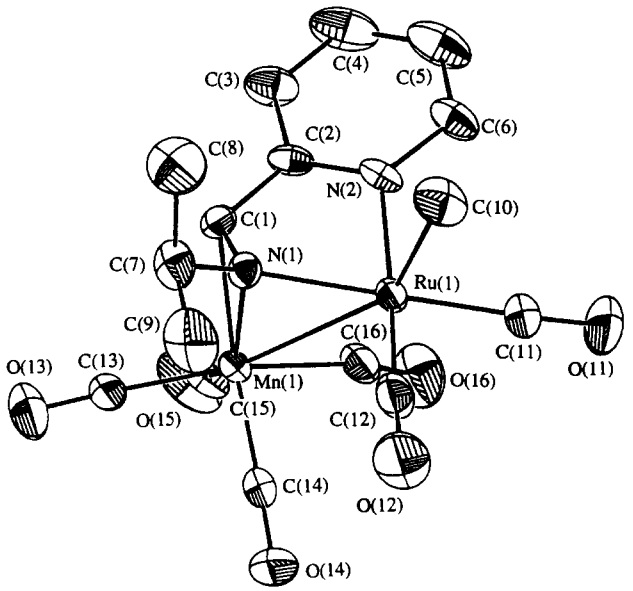


Fig. 3. ORTEP drawing of the molecular structure of [$(CO)_4$Mn-$\mu$-($\sigma$(N),$\sigma$(N'),$\eta^2$(CN)-$^i$Pr-PyCa)Ru(Me)$(CO)_2$].

somewhat shorter, and the Mn–carbonyl bond lengths somewhat longer, than those in the starting complex.

### 3.3. Quantum yields

The efficiency of the photoreactions at different temperatures and irradiation wavelengths was established by quantum yield determinations. Quantum yields for the disappearance of the parent complex were determined in $CH_2Cl_2$ and $CHCl_3$. Both solvents have been shown to be radical scavengers, and they gave rise to the photochemically and thermally-stable photoproducts [Mn(Cl)$(CO)_5$] and [Ru(Cl)(Me)$(CO)_2$($\alpha$-diimine)]. For comparison, quantum yields were also determined for the photoreactions with the radical scavenger 9,10-phenanthrenequinone (9,10-phenQ) and with $PPh_3$ in THF. The quantum yields (Table 6) in $CHCl_3$ are somewhat higher than in $CH_2Cl_2$ owing to the fact that the former solvent is a better radical scavenger. Table 6 also shows that the quantum yields increase by at least a factor of 2 on going from 514.5 nm to 457.9 nm excitation, and decrease upon lowering the temperature from 293 K to 233 K. The most remarkable observation is the much lower quantum yield observed for the MnRuPyCa complex. An explanation for this effect will be presented in the Discussion.

### 3.4. ESR spectra

The formation of radicals by homolysis of the Mn–Ru bond was confirmed by the ESR spectra obtained by irradiation of the two complexes. Fig. 4(a) shows the ESR spectrum of the radical [Ru(Me)$(CO)_2$($^i$Pr-PyCa)]$^\cdot$ in toluene at room temperature. The spectrum consists of overlapping signals due to the hyperfine coupling with one ruthenium and two nitrogen nuclei. Simulation of this ESR spectrum was performed with one Ru ($I = 5/2$; $a_{Ru} = 4.70$ G), two nitrogen ($I = 1$; $a_N = 6.62$ G) and one imine-H ($I = 1/2$; $a_H = 1.39$ G). For the corresponding [Ru(Me)$(CO)_2$($^i$Pr-DAB)]$^\cdot$ radical, the spectrum could be simulated with one Ru ($I = 5/2$; $a_{Ru} = 2.45$ G) and two nitrogen ($I = 1$; $a_N = 10.50$ G) nuclei. The coupling constant for the two imine protons is probably smaller than the observed line width (1.28 G), since no effect from these nuclei could be observed. The same holds for the coupling

Table 6
Quantum yields ($\Phi$) for the disappearance of MnRuDAB and MnRuPyCa. Dependence on the radical scavenger, the temperature and the irradiation wavelength (estimated error 5%)

| $\lambda_{exc}$ (nm) | Temperature (K) | Solvent | Quantum yield ($\Phi$) | |
|---|---|---|---|---|
| | | | MnRuDAB | MnRuPyCa |
| 514.5 | 293 | $CH_2Cl_2$ | 0.34 | 0.045 |
| 501.7 | 293 | $CH_2Cl_2$ | 0.33 | 0.055 |
| 488.0 | 293 | $CH_2Cl_2$ | 0.38 | 0.065 |
| 476.5 | 293 | $CH_2Cl_2$ | 0.39 | 0.086 |
| 457.9 | 293 | $CH_2Cl_2$ | 0.73 | 0.11 |
| 514.5 | 293 | $CHCl_3$ | 0.49 | 0.078 |
| 514.5 | 273 | $CHCl_3$ | 0.36 | 0.073 |
| 514.5 | 253 | $CHCl_3$ | 0.36 | 0.067 |
| 514.5 | 233 | $CHCl_3$ | 0.37 | 0.059 |
| 514.5 | 293 | THF + phenQ | 0.30 | 0.06 |
| 514.5 | 293 | THF + $PPh_3$ | 0.38 | 0.05 |

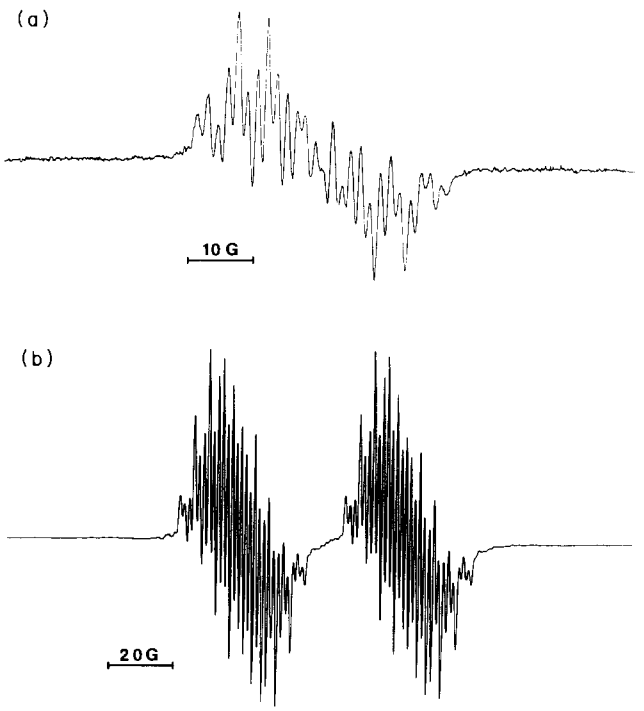


Fig. 4. ESR spectra of (a) [Ru(Me)(S)$(CO)_2$($^i$Pr-PyCa)]$^\cdot$ and (b) [Ru(Me)$(PPh_3)(CO)_2$($^i$Pr-PyCa)]$^\cdot$ in toluene at room temperature.

with the H nuclei of the methyl ligand. The large nitrogen coupling constants observed for both radicals indicate that the unpaired electron is mainly localized on the α-diimine ligand. A similar conclusion was derived from the ESR spectra of the radicals $[Mn(CO)_3(^tBu\text{-}DAB)]^{\cdot}$, $[Re(CO)_3(\alpha\text{-diimine})]^{\cdot}$ and $[Cr(CO)_4(\alpha\text{-diimine})]^{-}$ [6,33,34]. As indicated by the values of $a_{Ru}$ and $a_N$, this localization increases on going from the $^i$Pr–PyCa to the $^i$Pr-DAB radical complex.

The ESR detection of organometallic radicals without using a spin trap normally requires localization of the unpaired electron in a low-lying ligand orbital. Thus, the semiquinone radicals $[Ru(L)(PPh_3)(CO)_2(o\text{-}O_2C_6Cl_4^{\cdot})]^{n+}$ [L = $PPh_3$ ($n = 1$), halide ($n = 0$)] [35] could be observed as persistent radicals, whereas the metal-centred radicals $[RuCp(CO)_2]^{+\cdot}$ [36] and $[Ru(SiMe_3)(CO)_4]^{+\cdot}$ [37] could only be detected by using a spin trap. The natural isotopes $^{99}$Ru and $^{101}$Ru (both $I = 5/2$) can give rise to different hyperfine coupling constants provided that the difference in $a_{Ru}$ between these two isotopes is larger than the line width. This was the case for the radicals $[RuCp(CO)_2]^{+\cdot}$ [36] and $[Ru(L)(PPh_3)(CO)_2(o\text{-}O_2C_6Cl_4^{\cdot})]^{n+}$ [35] but not for the radicals under study.

The coordinatively unsaturated character of the radicals $[Ru(Me)(CO)_2(\alpha\text{-diimine})]^{\cdot}$ became evident when $PPh_3$ was added to the solution before irradiation. The ESR spectra then showed the presence of the radical adducts $[Ru(Me)(PPh_3)(CO)_2(\alpha\text{-diimine})]^{\cdot}$ with $^{31}$P coupling ($I = 1/2$). The ESR spectrum of the $^i$Pr-DAB radical could be simulated with coupling to one Ru ($a_{Ru}$ = 2.02 G) and one phosphorus nucleus ($a_P$ = 72.67 G), and two nitrogen nuclei ($a_N$ = 7.74 G). For this adduct also the coupling constants for the imine and methyl hydrogens are probably smaller than the line width (1.30 G). For the corresponding adduct $[Ru(Me)(PPh_3)(CO)_2(^i\text{Pr-PyCa})]^{\cdot}$ [See Fig. 4(b)] simulation was performed with one Ru ($a_{Ru}$ = 3.03 G) and one phosphorus nucleus ($a_P$ = 52.11 G), two nitrogens ($a_N$ = 4.33 G) and one imine H ($a_H$ = 1.20 G). Similar radical adducts $[Re(L)(CO)_3(^t\text{Bu-DAB})]^{\cdot}$ appeared to be formed upon irradiation of $[Ph_3Sn—Re(CO)_3(^t\text{Bu-DAB})]$ in the presence of L = $PR_3$ or pyridine [34].

### 3.5. Low-temperature reactions

The photoreactions of the complexes were also studied at low temperatures in 2-MeTHF. The IR and UV–vis data for the photoproducts thus obtained are listed in Table 7. Cooling the solution to 133 K hardly changed the carbonyl stretching frequencies of the starting complexes. Thus, the ν(CO) bands of Mn-RuDAB merely shifted from 2055, 1995, 1966 and 1948 $cm^{-1}$ to 2054, 1989, 1962 and 1948 $cm^{-1}$.

At temperatures ≥ 193 K, irradiation of Mn-RuDAB gave the same photoproducts, viz. $[Mn_2(CO)_{10}]$ and $[Ru(Me)(CO)_2(^i\text{Pr-DAB})]_2$ as were obtained at room temperature. However, irradiation of MnRuPyCa at 193 K only produced a small amount of photoproduct A, probably a C–C-coupled dimer, formed at room temperature. Instead, the main products at this tem-

Table 7
IR and UV–vis data for the photoproducts obtained various solvents at low temperature [ν(CO)in $cm^{-1}$, $\lambda_{max,abs}$ in nm]

| Temperature (K) | Solvent | Product | ν(CO) | $\lambda_{max,abs}$ |
|---|---|---|---|---|
| 193 | 2-MeTHF | $[Mn_2(CO)_{10}]$ | 2045, 2009, 1981 | 337 |
| | | photoproduct A | 2027, 1954 | – |
| | | $[Ru(Me)(CO)_2(^i\text{Pr-PyCa})]_2$ | 1973, 1946, 1913 | 837 |
| 193 | 2-MeTHF | $[Mn_2(CO)_{10}]$ | 2045, 2009, 1981 | 337 |
| | | $[Ru(Me)(CO)_2(^i\text{Pr-DAB})]$ | 1981, 1953, 1922 | 732 |
| 133 | 2-MeTHF | $[Mn_2(CO)_{10}]$ [a] | 2043, 2006, 1980 | 337 |
| | | $[Ru(Me)(S)(CO)_2(^i\text{Pr-PyCa})]^+$ | 2032, 1960 | |
| | | $[Mn(CO)_5]^-$ | 1897, 1862, 1956 (sh) | – |
| 133 | 2-MeTHF | $[Mn_2(CO)_{10}]$ [a] | 2043, 2007, 1976 | – |
| | | $[Ru(Me)(S)(CO)_2(^i\text{Pr-DAB})]^+$ | 2031, 1957 | 350 |
| | | $[Mn(CO)_5]^-$ | 1897, 1862, 1957 (sh) | |
| 143 | 2-Cl-butane | $[Mn_2(CO)_{10}]$ [a] | | |
| | | $[Ru(Me)(S)(CO)_2(^i\text{Pr-PyCa})]^{+}$ [b] | | |
| | | $[Mn(CO)_5]^{-}$ [b] | | |
| 143 | 2-Cl-butane | $[Mn_2(CO)_{10}]$ [a] | 2045, 2010, 1981 | – |
| | | $[Ru(Me)(S)(CO)_2(^i\text{Pr-DAB})]^{+}$ [b] | 2028, 1952 | 320 |
| | | $[Mn(CO)_5]^{-}$ [b] | 1890, 1867, 1842 | – |

[a] Minor product.
[b] In contact ion pair.

perature were the metal–metal-bonded dimers [Ru(Me)(CO)$_2$($^i$Pr-PyCa)]$_2$ and [Mn$_2$(CO)$_{10}$], just as for the $^i$Pr-DAB complex. This Ru dimer was characterized by its intense absorption band at 837 nm and IR $\nu$(CO) bands at 1973, 1946 and 1913 cm$^{-1}$. [Mn$_2$(CO)$_{10}$] was identified by its well known $\nu$(CO) bands and the $\sigma_b \rightarrow \sigma^*$ transition at 337 nm [27].

In order to account for the influence of the temperature on product formation, the product mixture from MnRuPyCa at 193 K was raised in temperature. The IR bands of both dimers then slowly disappeared and the starting complex was re-formed. Apparently, since [Mn$_2$(CO)$_{10}$] is thermally stable, the Ru dimer decomposes into radicals at higher temperatures. These radicals then react with [Mn$_2$(CO)$_{10}$] to give the parent complex.

The occurrence of this back-reaction is certainly responsible for the relatively small quantum yields obtained for this complex (Table 6). Evidently, most of the radicals formed at room temperature do not produce the unknown photoproduct A, but combine with one another to give the parent complex.

Irradiation of the complexes in 2-MeTHF at still lower temperatures ($133 \leq T \leq 163$ K) gave the ionic species [Mn(CO)$_5$]$^-$ and [Ru(S)(Me)(CO)$_2$($\alpha$-diimine)]$^+$ (S = 2-MeTHF) in addition to a small amount of [Mn$_2$(CO)$_{10}$] and [Ru(Me)(CO)$_2$($\alpha$-diimine)]$_2$. The ions were characterized by their $\nu$(CO) stretching frequencies (see Table 7) [38]. A similar photodisproportionation into ions was observed for 2-chlorobutane at 143 K. In this case, however, the cation could not be stabilized by a coordinating solvent and, instead of the solvent-separated ion pair, a contact-ion pair (CIP) [Mn(CO)$_5^-$ $\cdots$ Ru(Me)(CO)$_2$($\alpha$-diimine)$^+$] was formed. Formation of this CIP was accompanied by a shift of the lowest $\nu$(CO) of [Mn(CO)$_5$]$^-$ from 1857 cm$^{-1}$ to 1842 cm$^{-1}$. This shift is caused by the weak coordination of a CO ligand of this anion to the cation. A similar effect has been observed for the CIPs [Mn(CO)$_5^-$ $\cdots$ Na$^+$] [39,40] and [Mn(CO)$_5^-$ $\cdots$ Re(CO)$_3$(bpy′)$^+$] [38]. In the latter case, the CIP appeared to be formed by homolysis of the metal–metal bond of [(CO)$_5$Mn–Re(CO)$_3$(bpy′)] followed by an electron-transfer (ET) reaction, and not by heterolysis of the metal–metal bond since the ion-pair formation was completely quenched by addition of a radical scavenger.

Unlike the reactions of the analogous [(CO)$_5$Mn–Mn(CO)$_3$($\alpha$-diimine)] [6,12,13] complexes, no reaction inducing CO loss was observed for MnRuDAB and MnRuPyCa at these low temperatures. This difference in behaviour is due to the fact that the LF state, from which such a CO loss reaction takes place, is lower in energy for the first-row transition metals than for those in the second and third row. As a result, irradiation of the complexes under study into their Ru $\rightarrow$ $\alpha$-diimine (MLCT) transitions did not lead to population of a reactive LF state of the Ru fragment.

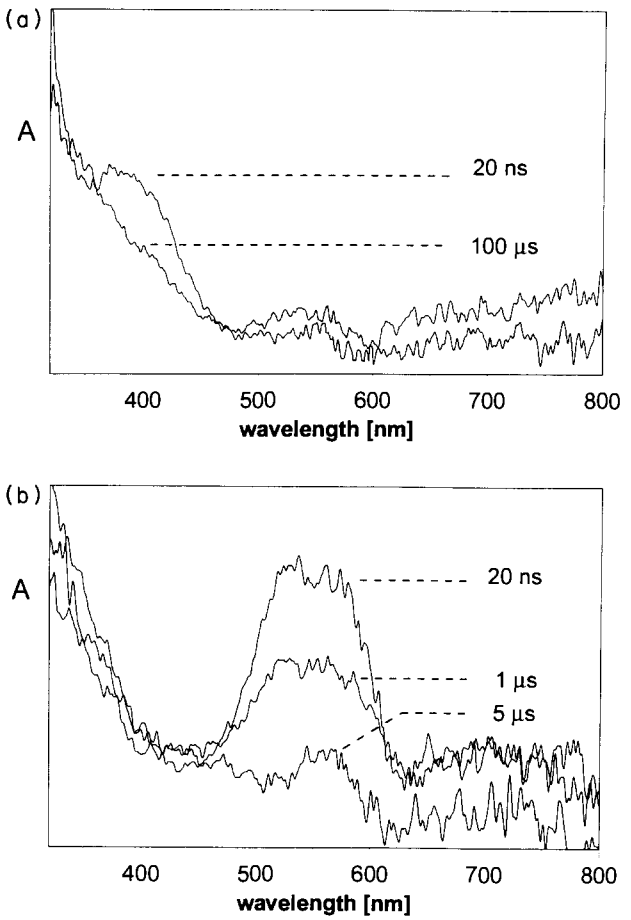


Fig. 5. Transient absorption spectra obtained by irradiation of MnRuDAB with a 532 nm pulse of an Nd:YAG laser in (a) THF and (b) hexane, both at room temperature. The spectra are corrected for the disappearance of the parent complex.

### 3.6. Flash photolysis

In order to establish the primary photoprocess, nanosecond transient absorption spectra were measured upon excitation of MnRuPyCa and MnRuDAB in THF and hexane. For both complexes the disappearance of the MLCT band indicated that the initial complex had been consumed upon photolysis. The MnRuDAB complex after 0.1 ms showed ca. 10% recovery compared with the initial depletion. For MnRuPyCa, on the other hand, half of the original depletion had disappeared after 0.1 ms. This confirms the indication from the low-temperature and quantum yield measurements that most of the radicals formed by irradiation of MnRuPyCa combine with one another to regenerate the parent complex.

The transient absorption spectra generated from MnRuDAB strongly depended on the solvent used. Figs. 5(a) and (b) show these spectra in THF and

hexane, respectively, after correction for the disappearance of the initial complex. The transient spectrum in THF only showed absorption in the visible region within the laser pulse, which was then immediately converted into a long-lived (> 0.1 ms) species which absorbed near 300 nm. This latter absorption is assigned to the solvated $[Ru(Me)(THF)(CO)_2(^iPr\text{-}DAB)]^\cdot$ radical by similarity of the absorption spectrum to that of the electrochemically generated $[Ru(Me)(PrCN)(CO)_2(^iPr\text{-}DAB)]^\cdot$ [29]. For MnRuPyCa, similar data were obtained.

In hexane, on the other hand, a long-lived intermediate was observed which had its maximum at about 550 nm. This intermediate was converted within 5 μs into a species with absorptions similar to those observed in THF.

### 3.7. Reactions in the presence of a Lewis base

When the photoreactions were performed in the presence of a strongly coordinating ligand such as phosphine, ions were formed even at room temperature. Thus, irradiation of MnRuDAB in the presence of $P(^nBu)_3$ gave rise to $[Mn(CO)_5]^-$, $[Ru(Me)(P(^nBu)_3)(CO)_2(^iPr\text{-}DAB)]^+$ and the monocarbonyl cation $[Ru(Me)(P(^nBu)_3)_2(CO)(^iPr\text{-}DAB)]^+$. When, instead of $P(^nBu)_3$, $P(OMe)_3$ was added to the solution, only the monocarbonyl cation $[Ru(Me)(P(OMe)_3)_2(CO)(^iPr\text{-}DAB)]^+$ was formed. The products of these reactions were characterized by comparing their IR frequencies (collected in Table 8) with those of the cations obtained spectroelectrochemically from the corresponding halides $[Ru(X)(R)(CO)_2(\alpha\text{-diimine})]$ [29].

The reactions were completely quenched by radical scavengers and the cations are therefore formed by electron transfer from the $[Ru(Me)(PR_3)(CO)_2(^iPr\text{-}DAB)]^\cdot$ radicals to $[Mn(CO)_5]^\cdot$ or $[Mn_2(CO)_{10}]$. In the case of $P(OMe)_3$, the cations $[Ru(Me)(P(OMe)_3)(CO)_2(^iPr\text{-}DAB)]^+$ were apparently not stable in the presence of an excess of the ligand and reacted further to give the monocarbonyl cations. In most cases, the electron-transfer reaction was not complete since small amount of the radicals could still be detected (Table 8). Upon treatment with harder bases such as pyridine (Py) or $NEt_3$, disproportionation was only observed when high concentrations of the base were used.

A similar influence of the hardness of the base on the electron-transfer reaction has been observed for the corresponding $[(CO)_5Mn\text{–}Mn(CO)_3(\alpha\text{-diimine})]$ complexes [41]. This effect was in the latter case ascribed to the inability of the hard bases to coordinate effectively to the $[Mn(CO)_3(\alpha\text{-diimine})]^\cdot$ radicals. In contrast to these Mn–Mn-bonded complexes, the photodisproportionation reactions under study were not catalytic since the quantum yields never exceeded unity.

In connection with these electron-transfer reactions, attention was paid to the initiation of substitution reactions by electron transfer from these radicals [41–43]. For this purpose, the substitution of CO in $[Ru_3(CO)_{12}]$ by a Lewis base L (P- or N-donor ligand) was studied in the absence and presence of MnRuDAB and MnRuPyCa (MnRu/$[Ru_3(CO)_{12}]$/L = 1:20:100). The radicals formed from MnRuDAB did not initiate these reactions, but the radicals $[Ru(Me)(L)(CO)_2(^iPr\text{-}PyCa)]^\cdot$ (L = $PPh_3$, $P(c\text{-}Hex)_3$, $P(OMe)_3$ and pyridine) were capable of so doing and gave rise to the formation of $[Ru_3(L)(CO)_{11}]$. This result is not surprising, since the radical complex $[Ru(Me)(PPh_3)(CO)_2(^iPr\text{-}PyCa)]^\cdot$, for example, is more reducing ($E_p^c = -2.35$ V) than the corresponding $^iPr$-DAB radical ($E_p^c = -2.23$ V) [29].

Table 8
IR data for the photoproducts obtained upon reaction with P- and N-donor ligands at room temperature in THF [ν(CO) in $cm^{-1}$]

| Donor ligand | Photoproducts | ν(CO) $^iPr$-DAB complex | ν(CO) $^iPr$-PyCa complex |
|---|---|---|---|
| | $[Mn(CO)_5]^-$ | 1893, 1865 1849 (sh) | 1893, 1865 1849 (sh) |
| $P(^nBu)_3$ | $[Ru(Me)(P(^nBu)_3)(CO)_2(\alpha\text{-diimine})]^+$ | 2030, 1956 | 2036, 1969 |
| | $[Ru(Me)(P(^nBu)_3)_2(CO)(\alpha\text{-diimine})]^\cdot$ | 1944 | 1937 |
| | $[Ru(Me)(P(^nBu)_3)(CO)_2(\alpha\text{-diimine})]^\cdot$ | 2005, 1939 | |
| $PPh_3$ | $[Ru(Me)(PPh_3)(CO)_2(\alpha\text{-diimine})]^+$ | | 2043, 1984 |
| | $[Ru(Me)(PPh_3)(CO)_2(\alpha\text{-diimine})]^\cdot$ | 2009, 1943 | |
| $P(OMe)_3$ | $[Ru(Me)(P(OMe_3)_2(CO)(\alpha\text{-diimine})]^+$ | – | 1975 |
| | $[Ru(Me)(P(OMe_3)_2(CO)(\alpha\text{-diimine})]^\cdot$ | 1946 | – |
| Py | $[Ru(Me)(Py)(CO)_2(\alpha\text{-diimine})]^+$ | 2028, 1968 | 2041, 1973 |
| | $[Ru(Me)(CO)_2(^iPr\text{-}DAB)]_2$ | 1981, 1952, 1920 | – |
| $NEt_3$ | $[Ru(Me)(CO)_2(^iPr\text{-}DAB)]_2$ | 1982, 1953, 1925 | – |
| | photoproduct A | – | 2024, 1960 |
| | $[Ru(Me)(NEt_3)(CO)_2(\alpha\text{-diimine})]^\cdot$ | – | 2009, 1942 |

## 4. Discussion

The formation of the dimers $[Mn_2(CO)_{10}]$ and $[Ru(Me)(CO)_2(^iPr\text{-}DAB)]_2$, the quenching of the reactions by radical scavengers and the detection of $[Ru(Me)(CO)_2(\alpha\text{-diimine})]^\cdot$ radicals by ESR spectroscopy clearly shows that homolysis of the Mn — Ru bond is the primary photoprocess of the complexes MnRuDAB and MnRuPyCa.

The two complexes differ, however, in the nature of the product at room temperature. The $[Ru(Me)(CO)_2(^iPr\text{-}DAB)]^\cdot$ radicals dimerized to give $[Ru(Me)(CO)_2(^iPr\text{-}DAB)]_2$. The corresponding $[Ru(Me)(CO)_2(^iPr\text{-}PyCa)]^\cdot$ radicals only dimerized at lower temperatures. At room temperature, the dimer is not stable thermally and the radicals react back with $[Mn(CO)_5]^\cdot$ and $[Mn_2(CO)_{10}]$ to give the parent complex. A small portion formed an as yet unidentified photoproduct A, which might be a C–C-coupled dimer. The occurrence of the back-reaction became evident when the solutions of products obtained by low-temperature photolysis were raised in temperature and when the absorption spectra of the transients were monitored over a period of 0.1 ms after a laser pulse.

Importantly, the above-mentioned dimers were only obtained as main photoproducts in coordinating solvents such as THF. The main photoproducts in hexane were the $\alpha$-diimine-bridged complexes $[(CO)_3Mn\text{-}\mu\text{-}(\sigma(N),\sigma(N'),\eta^2(CN),\eta^2(CN')\text{-}^iPr\text{-}DAB)Ru(Me)(CO)_2]$ and $[(CO)_4Mn\text{-}\mu\text{-}(\sigma(N),\sigma(N'),\eta^2(CN)\text{-}^iPr\text{-}PyCa)Ru(Me)(CO)_2]$. Similar products have been obtained upon photolysis of the corresponding complexes $[(CO)_5Mn—Mn(CO)_3(\alpha\text{-diimine})]$ [6] and $[(CO)_5Mn—Mn(CO)_3(DBSD)]$ (DBSD = di-t-butylsulphurdiimine) [32]. Just as for those complexes, formation of the products was prevented by radical scavengers and accelerated in the presence of extra $[Mn(CO)_5]^\cdot$ radicals. This means that these products are not formed by CO loss as the primary photoprocess, but by a radical-coupling reaction of the $[Mn(CO)_5]^\cdot$ and $[Ru(Me)(CO)_2(\alpha\text{-diimine})]^\cdot$ radicals. The formation of these products is not unexpected since a radical-coupling reaction will take place between the metal centre of the $[Mn(CO)_5]^\cdot$ radical and the $\alpha$-diimine radical anion of the $[Ru(Me)(CO)_2(\alpha\text{-diimine})]^\cdot$ radical complex. This reaction apparently leads to bond formation between Mn and the reactive imine group of the $\alpha$-diimine, with concomitant loss of CO and formation of a metal–metal bond. In the case of MnRuDAB, the $[(CO)_4Mn\text{-}\mu\text{-}(\sigma(N),\sigma(N'),\eta^2(CN)\text{-}^iPr\text{-}DAB)Ru(Me)(CO)_2]$ product appeared to be an unstable intermediate that leads to formation of the stable photoproduct $[(CO)_3Mn\text{-}\mu\text{-}(\sigma(N),\sigma(N'),\eta^2(CN),\eta^2(C'N')\text{-}^iPr\text{-}DAB)Ru(Me)(CO)_2]$. The mechanism of this reaction is depicted schematically in Scheme 1.

The question remains as to why the radicals dimerize in THF and react with each other in hexane to give these $\alpha$-diimine-bridged photoproducts. Apparently, the radicals do not diffuse in hexane. It is unlikely that the radicals are simply trapped within the solvent cage when dissolved in hexane, since THF and hexane do not differ so much in their viscosity at room temperature. It is, however, possible that the radical pair, formed after homolysis of the Mn—Ru bond, does not decompose so easily in hexane as in THF but instead gives rise to the observed radical-coupling reaction. Another possibility is that in hexane no splitting of the metal–metal bond occurs from the $^3\sigma_b\pi^*$ state and that at least part of the photoproduct is formed by intramolecular transfer of the $Mn(CO)_5$ group to the radical anion [11].

The emission lifetime of this state has recently been measured for MnRuDAB and MnRuPyCa in a 2-

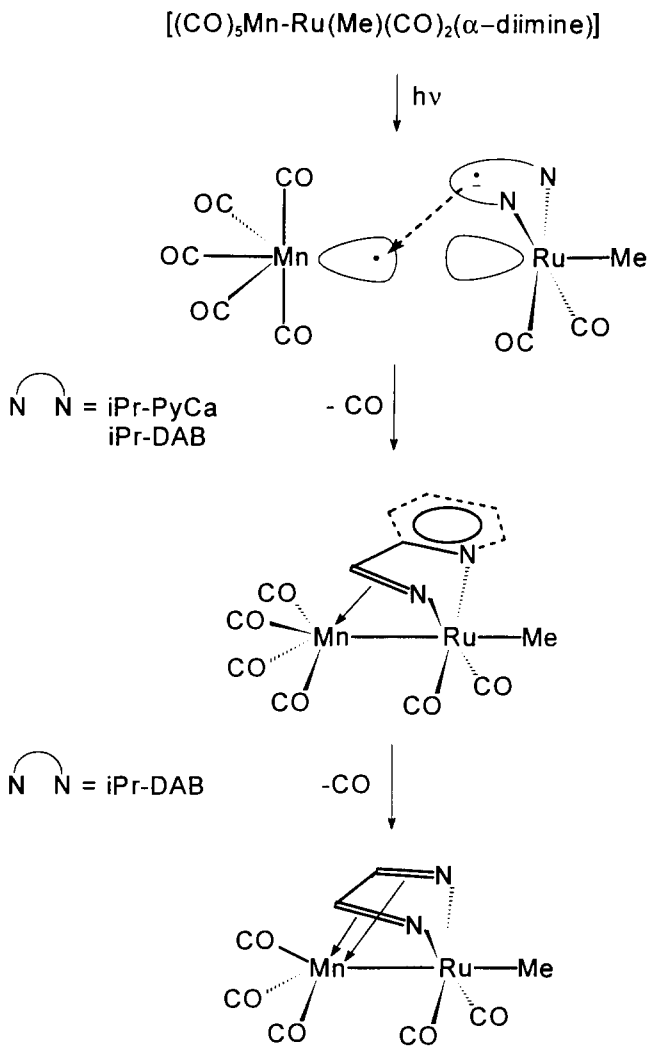


Scheme 1. Proposed reaction scheme for the formation of photoproducts $[(CO)_4Mn\text{-}\mu\text{-}(\sigma(N),\sigma(N'),\eta^2(CN)\text{-}^iPr\text{-}PyCa)Ru(Me)(CO)_2]$ and $[(CO)_3Mn\text{-}\mu\text{-}(\sigma(N),\sigma(N'),\eta^2(CN),\eta^2(C'N')\text{-}^iPr\text{-}DAB)Ru(Me)(CO)_2]$.

MeTHF glass at 77 K [19]. The lifetime of 10 $\mu$s measured for MnRuDAB agrees with that of a few microseconds at room temperature derived from the transient absorption spectra in hexane [Fig. 5(b)]. This transient absorption is therefore assigned to the $^3\sigma_b\pi^*$ state. The solvent has, apparently, a large influence on the lifetime of this state, since in THF this transient could only be observed within the laser pulse ($\tau \leq 10$ ns). This solvent dependence has already been shown to be a characteristic property of such a $^3\sigma_b\pi^*$ state in the case of [Re(benzyl)(CO)$_3$($^i$Pr-DAB)] [9]. For that complex the lifetime of the $^3\sigma_b\pi^*$ state was found to be less than 10 ns in THF and about 280 ns in toluene. This solvent effect is probably due to the specific bonding properties of these complexes in their $^3\sigma_b\pi^*$ state. In this state, the Mn—Ru bond is weakened with respect to the ground state but it still contains one electron in the $\sigma_b$(Mn—Ru) orbital. In a coordinating solvent such as THF, this weak bond will be broken more easily than in hexane, and this effect could be responsible for the observed solvent dependence of the lifetime.

## 5. Conclusions

Irradiation of the complexes MnRuDAB and MnRuPyCa into their MLCT bands gives rise to homolysis of the metal–metal bond from the reactive $^3\sigma_b\pi^*$ state, which has a strongly solvent-dependent lifetime.

The radicals formed give different photoproducts depending on the $\alpha$-diimine, the temperature and the solvent used. The influence of the temperature and the solvent is directly connected with the coordination of the solvent to the 16e radical complexes [Ru(Me)(CO)$_2$($\alpha$-diimine)]$^\cdot$ Upon solvent coordination, the radicals may dimerize, react with each other to regenerate the parent complex, or undergo an electron-transfer reaction with formation of ion pairs. In non-coordinating solvents on the other hand, the Mn and Ru radicals react with each other to give the ligand-bridged complexes [(CO)$_3$Mn-$\mu$-($\sigma$(N),$\sigma$(N′),$\eta^2$(CN),$\eta^2$(C′N′)-$^i$Pr-DAB)Ru(Me)(CO)$_2$] and [(CO)$_4$Mn-$\mu$-($\sigma$(N),$\sigma$(N′),$\eta^2$(CN)-$^i$Pr-PyCa)Ru(Me)(CO)$_2$], as shown by the X-ray structure determination for the latter complex.

## Acknowledgement

We thank J. Fraanje for collecting the X-ray diffraction data and the Netherlands Foundation for Chemical Research (SON) and the Netherlands Organization for Pure Research (NWO) for financial support.

## References

[1] D.J. Stufkens, in I. Bernal (ed.), *Stereochemistry of Organometallic and Inorganic Compounds*, Elsevier, Amsterdam, 1989, Vol. 3, p. 226.
[2] D.J. Stufkens, *Coord. Chem. Rev., 104* (1990) 39.
[3] M.W. Kokkes, D.J. Stufkens and A. Oskam, *Inorg. Chem., 24* (1985) 2934.
[4] M.W. Kokkes, W.G.L. de Lange, D.J. Stufkens and A. Oskam, *J. Organomet. Chem., 294* (1985) 59.
[5] M.W. Kokkes, D.J. Stufkens and A. Oskam, *Inorg. Chem., 24* (1985) 4411.
[6] T. van der Graaf, D.J. Stufkens, A. Oskam and K. Goubitz, *Inorg. Chem., 30* (1991) 299.
[7] D.L. Morse and M.S. Wrighton, *J. Am. Chem. Soc., 98* (1976) 3931.
[8] T.J. Meyer and J.V. Caspar, *Chem. Rev., 85* (1985) 187.
[9] B.D. Rossenaar, C.J. Kleverlaan, D.J. Stufkens and A. Oskam, *J. Chem. Soc., Chem. Commun.*, (1994) 63.
[10] H.A. Nieuwenhuis, M.C.E. van de Ven, D.J. Stufkens and A. Oskam, *Organometallics, 14* (1995) 720.
[11] K. Kaupp, H. Stoll, H. Preuss, W. Kaim, T. Stahl, G. van Koten, E. Wissing, W.J. Smeets and A.L. Spek, *J. Am. Chem. Soc., 113* (1991) 5606.
[12] R.R. Andréa, D.J. Stufkens and A. Oskam, *Inorg. Chem., 28* (1989) 318.
[13] B.D. Rossenaar, T. van der Graaf, R. van Eldik, C.H. Langford, D.J. Stufkens and A. Vlček, Jr., *Inorg. Chem., 33* (1994) 2865.
[14] G.J. Stor, S.L. Morrison, D.J. Stufkens and A. Oskam, *Organometallics, 13* (1994) 2641.
[15] P. Chen, T.D. Westmoreland, E. Danielson, K.S. Schanze, D. Anthon, P.E. Neveux, Jr. and T.J. Meyer, *Inorg. Chem., 26* (1987) 1116.
[16] K.S. Schanze, D.B. MacQueen, T.A. Perkins and L.A. Cabana, *Coord. Chem. Rev., 122* (1993) 63.
[17] T.A. Perkins, W. Humer, T.L. Netzel and K.S. Schanze, *J. Phys. Chem., 94* (1990) 2229.
[18] H.A. Nieuwenhuis, A. van Loon, M.A. Moraal, D.J. Stufkens, A. Oskam and K. Goubitz, *Inorg. Chim. Acta, 232* (1995) 19.
[19] H.A. Nieuwenhuis, D.J. Stufkens and A. Vlček, Jr., *Inorg. Chem.*, submitted for publication.
[20] Aberchromics Ltd., School of Chemistry and Applied Chemistry, University College of Cardiff, University of Wales.
[21] N. Walker and D. Stuart, *Acta Crystallogr., A39* (1983) 158.
[22] W.H. Zachariasen, *Acta Crystallogr., A23* (1967) 558.
[23] A.C. Larson, in F.R. Ahmed, S.R. Halt and C.P. Huber (eds.), *The Inclusion of Secondary Extinction in Least-Squares Refinement of Crystal Structures Crystallographic Computing*, Munkgaard, Copenhagen, 1969, 29.
[24] D.T. Cromer and J.B. Mann, *Acta Crystallogr., A24* (1968) 321.
[25] *International Tables for X-ray Crystallography*, The Kynoch Press, Birmingham, UK, 1974, Vol. IV, p. 55.
[26] S.R. Hall, H.D. Flack and J.M. Stewart, (eds.) *XTAL3.2 Reference Manual*, Universities of Western Australia, Geneva and Maryland, 1992.
[27] N. Flitcroft, D.K. Huggins and H.D. Kaesz, *Inorg. Chem., 3* (1964) 1123.
[28] H. tom Dieck, W. Rohde and U. Behrens, *Z. Naturforsch., Teil B, 44* (1989) 158.
[29] H.A. Nieuwenhuis, F. Hartl and D.J. Stufkens, to be published.
[30] M.J.A. Kraakman, *Thesis*, University of Amsterdam, 1992.
[31] P.C. Servaas, G.J. Stor, D.J. Stufkens and A. Oskam, *Inorg. Chim. Acta, 178* (1990) 185.
[32] C. Mahabiersing, W.G.J. de Lange, K. Goubitz and D.J. Stufkens, *J. Organomet. Chem., 461* (1993) 127.
[33] H. tom Dieck, *Chem. Ber., 108* (1975) 163.
[34] R. Andréa, W.G.J. de Lange, T. van der Graaf, M. Rijkhoff,

D.J. Stufkens and A. Oskam, *Organometallics, 7* (1988) 1100.
[35] N.G. Connelly, I. Manners, J.R.C. Protheroe and M.W. Whiteley, *J. Chem. Soc., Dalton Trans.*, (1984) 2713.
[36] S. Sostero, D. Rehorek, E. Polo and O. Traverso, *Inorg. Chim. Acta, 209* (1993) 171.
[37] A. Hudson, M.F. Lappert, P.W. Lednor, J.J. MacQuitty and B.K. Nicholson, *J. Chem. Soc., Dalton* Trans., (1981) 2159.
[38] T. van der Graaf, A. van Rooy, D.J. Stufkens and A. Oskam, *Inorg. Chim. Acta, 187* (1991) 133.
[39] C.D. Pribula and T.L. Brown, *J. Organomet. Chem., 71* (1974) 415.
[40] M. York Darensbourg, D.J. Darensbourg, D. Burns and D.A. Drew, *J. Am. Chem. Soc., 98* (1976) 3127.
[41] T. van der Graaf, R. Hofstra, P.G.M. Schilder, M. Rijkhoff, D.J. Stufkens and J.G.M. van der Linden, *Organometallics, 10* (1991) 3668.
[42] M.I. Bruce, J.G. Matisons and B.K. Nicholson, *J. Organomet. Chem., 247* (1983) 321.
[43] M.I. Bruce, D.C. Kehoe, J.G. Matisons, B.K. Nicholson, P.H. Rieger and M.L. Williams, *J. Chem. Soc., Chem. Commun.*, (1982) 422.